


## PAPER

# Histopathological Image Classification Using Convolutional Neural Networks for Detection of Metastatic Breast Cancer in Lymph Nodes

Diego Alberto Cadillo-Laurentt, Ernesto Alonso Paiva-Peredo()

Universidad Tecnológica del Perú, Lima, Peru

[epaiva@utp.edu.pe](mailto:epaiva@utp.edu.pe)

## ABSTRACT

Breast cancer is currently one of the most diagnosed oncological diseases worldwide, with thousands of new cases per year. Early detection and identifying its progression are key to overcoming the mortality rate. A recurrent test, to determine how far the disease has spread throughout the patient's body, is the histological analysis of the sentinel lymph node near the breast. Although an expert pathologist performs this, it is usually an exhausting and time-consuming task, with a high possibility of error. This work presents a method to detect breast cancer metastasis through histological imaging of sentinel lymph nodes using convolutional neural networks. In this study, the performance of three models DenseNet-121, DenseNet-169 and DenseNet-201 are tested and compared. Experimental results indicated that the accuracy, precision, sensitivity and specificity (97.93%, 97.4%, 97.48% and 98.24%) of DenseNet-201 could reduce pathologist errors during the diagnostic process or serve as a second opinion tool.

## KEYWORDS

histopathology, image classification, convolutional neural networks, breast cancer

## 1 INTRODUCTION

Nowadays, the most proficient and efficient method for automatic image classification and recognition is based on convolutional neural networks (CNNs) [1]. It is mentioned in [2] that CNNs have performed well in medical image processing, mainly due to their effectiveness in extracting features. For example, in [3] they employ a DenseNet network together with a SENet to classify histopathological images of lymph nodes by applying data augmentation (rotate, invert, move, among other changes) to increase the training set in order to minimize overfitting. Multiclass classification with SENet is performed on the optimized parameters.

Cadillo-Laurentt, D.A., Paiva-Peredo, E.A. (2024). Histopathological Image Classification Using Convolutional Neural Networks for Detection of Metastatic Breast Cancer in Lymph Nodes. *International Journal of Online and Biomedical Engineering (iJOE)*, 20(2), pp. 31–45. <https://doi.org/10.3991/ijoe.v20i02.46789>

Article submitted 2023-09-12. Revision uploaded 2023-11-23. Final acceptance 2023-11-25.

© 2024 by the authors of this article. Published under CC-BY.

The experimental model with the best performance is MFSCNet A, in which the SENet block acquires information from the dense block channel and the transition layer of the DenseNet model. Similarly, in [4] they use an architecture based on DenseNet interleaved with SENet. For training and validation, use is made of the BreakHis dataset of 7909 (resized and normalized) images. The data augmentation technique is also applied to avoid overfitting. The developed model, called IDSNet, was able to outperform other compared models by 1 to 7%.

On the other hand, in [5] the authors have as a first stage the input of the images to the Faster R-CNN network, which delivers many false positives. Therefore, post processing is done to mitigate this problem through the extraction of appropriate features. Then, the post-processing outputs are input to the Resnet-50 and DenseNet-201 networks, so that in fourth stage, their final classification as a sample with or without mitosis is performed. As in [3], [4], data augmentation techniques are applied. The authors find that by applying the proposed model, they obtain 87.6% accuracy for the ICPR 2012 dataset and 84.8% for ICPR 2014.

Iqbal and Qureshi in [6] make use of the BreastUNet model to identify probably mitotic regions in histopathological images. Then these are classified into mitotic and non-mitotic nuclei. The model has as a first instance of cancer distinction the deep segmentation of instances. With this, probable mitotic parts are identified, which then with BreastUNet will be classified as mitotic and non-mitotic nuclei. It is important to note that the datasets of [6] were MITOS14, BreakHis as well as [4], BreCaHAD and TUPAC-16. [7] proposes a model called 6B-Net, which consists of 35 layers with a concurrent processing level. The network is first pre-trained to extract features, which then enter the feature selection algorithm of PSO and ACS. In parallel, a character vector is extracted using ResNet-50, similar to those performed in [5], [6]. The proposed method achieves 94.20% accuracy in classifying four classes of breast cancer and 90.10% accuracy in classifying eight classes of breast cancer.

Another very useful tool is the use of customized U-Net networks with dense connections, hopping connections, among others. According to [8], standard U-Nets are very good for medical computer vision tasks. [8] seeks to demonstrate that the design of a standard component model, with its larger architecture, mimics expert diagnostic procedures and can perform better diagnosis.

In [9], neural networks are used to identify ER/PR/HER2 status and histological type. A neural network capable of classifying images into 6 types of breast carcinoma is designed. The model was initialized with ImageNet weights and stochastically trained three times for each classification task. The network employed was Inceptionv3 with data augmentation during training. Model parameters including learning rate and batch size were initialized with values extracted from other networks designed to classify lung cancer. In contrast, a hybrid CNN composed of a recurrent unit controlled by another AlexNet is presented in [10]. A positive feature of the employed model is to use less computing resources compared to the network used in [9]. With the CNN AlexNet model, the authors propose to automatically extract features from the PCam dataset and identify samples with metastatic cancer. The updated PCam dataset is extracted from Kaggle, to which the data augmentation technique is applied before training. Finally, AlexNet-GRU [10] during the experiment phase proved to be more efficient than the CNN-GRU and CNN-LSTM models, achieving an accuracy of 99.50 %.

As expressed in multiple works reviewed in this section, not only is the chosen neural network model important, but also many other parameters that determine the training of the network are relevant [11]. As expressed in [12], the learning rate is the crucial hyperparameter used during the training of deep convolutional neural networks. That is why the authors emphasize the relevance of the dynamic learning rate over the fixed learning rate. It is important to specify that in [12], the range

of change of such rate is preset between lower and upper bounds, obtaining better accuracy in a smaller number of iterations and less loss. The authors using the triangular learning method achieved a validation accuracy of 91.84%, with lower epochs than the fixed learning rate counterparts.

It is important to know how noise can affect the effectiveness of image classifiers based on convolutional neural networks. Ademola et al. [13] warns that noise in images can have a significant impact on any type of classification, decreasing the degree of accuracy. In [14], [15], it is mentioned that it is a frequent problem in medical imaging and can have a significant effect on the results. Bayram et al [16] supports this claim, as in their experiments it was observed that the model accuracy decreases by 1.05% if no image processing technique is used. Furthermore, in [17], it is mentioned that pre-training the network on a larger data set helped to reduce the impact of noise.

As demonstrated in this section, convolutional neural networks are able to classify mammary lymph node images with an accuracy  $\geq 90\%$ . The negative counterpart of obtaining a high percentage of accuracy is the high training time and high consumption of computational resources. Many authors cited use a large number of epochs during training. Despite the search for optimization algorithms and the adjustment of the learning rate with multiple methods, they do not achieve a significant reduction in training time. The authors cited in this section mostly focus on modifying or combining existing CNNs to optimize the performance of the classifier model. However, the definition and adequate adjustment of the hyper parameters has a transcendental role in obtaining a high accuracy rate, during the review of previous bibliography, the lack of scientific studies that focus on the choice of the most adequate values has been identified, and with it the decrease of the training time and the obtaining of high accuracy rates.

## 2 METHODOLOGY

This section presents the models and methods used in this study. The DenseNet family architectures used, the weight allocation and optimization, the hyperparameters used to validate the model performance, the implementation environment and the dataset used are disclosed.

### 2.1 DenseNet architecture

In a DenseNet architecture, each layer is connected to all other layers, hence the name densely connected convolutional networks [18]. In the present research, the CNN architectures DenseNet-121, DenseNet-169 and DenseNet-201 will be employed. The three CNNs employed are pre-trained models, using the ImageNet database. The convolutional layer weights have been tuned to capture different types of edge patterns that can be easily reused for inference in other types of images.

### 2.2 Optimization methodology

In training, the hyperparameters of the model govern the process. They control the behavior during training and have a significant impact on the accuracy and convergence of the model. Leslie Smith in [19] proposed a technique for setting hyperparameters in complex models that optimizes time and effort, but improves performance. In this section, we discuss how the 1-cycle policy is employed within the present research work.

**1-cycle policy.** It is posited that, by monitoring the loss in validation and testing at the beginning of training, sufficient information is obtained to tune the architecture and hyperparameters. This eliminates the need to run random searches or run the rest of the training. This approach is based on the well-known concept of the trade-off between under-fitting and over-fitting, through the setting of learning rate (LR) and weight drop (WD).

**Learning rate finder.** In order to develop the 1-cycle policy, the maximum learning rate must first be defined. For this purpose, a learning rate finder is implemented. A way to estimate a good learning rate is described in [20]. During an epoch, an SGD is started with a very low learning rate, which changes in each mini-batch until it reaches a very high value. The loss decreases at first, then stops and increases again, usually very quickly. As recommended in [20], losses are plotted against learning rates on a logarithmic scale. A good learning rate would be in the range where the loss continues to decrease instants before the minimum, where the loss still improves.

**Search for weight decay.** Weight decay is not like learning rates, the best value should remain constant during training. Since the performance of the network depends on a suitable weight decay value, during experimentation we plot the learning rate range over three weight decay values in order to find the best learning rate with its respective weight decay. Leslie Smith [19], [20] proposes to select the largest WD that allows us to train at a high learning rate, so we do a manual logarithmic grid search with  $1e^{-2}$ ,  $1e^{-4}$  and  $1e^{-6}$  weight decays.

### 2.3 Tuning the reference model

Once the first training using the 1-cycle policy is completed, all parameters are saved and frozen. Then a more accurate tuning process or second training is applied, although the percentage of success is  $\geq 90\%$ , but this can be better. This process allows us to unfreeze all the trainable parameters of the model and improve them. For this second training, the 1-cycle policy is used again. Therefore, we must define a new optimal learning rate, in [19] it is mentioned that it must be much lower than the first one. The value of WD is constant during the whole training process.

According to the above, the convolutional neural network will be trained in two successive training stages. For practicality, we call the first stage as first tuning, and the second stage as final tuning.

### 2.4 Development environment

The experimentation is done in the environment provided by Kaggle, using the Python programming language [21]. Additionally, FastAI [22] was used to import the pretrained model, apply the 1-cycle policy, learning rate search and weight decays. FastAI is an open source deep learning library, built on top of PyTorch [23], which provides high-level APIs for training and applying deep machine learning models. PyTorch is an open source deep learning library based on Python.

### 2.5 Dataset

The Kaggle library dataset [24], is a filtered version of the PCam dataset. The only difference between these two is that all duplicate images have been removed. The collection contains 220025 images of sentinel lymph node histopathologic studies

from 162 women diagnosed with breast cancer. Each tissue sample is stained with H&E, examined using a x40 objective. For the creation of the array, x10 subsampling is used to increase the field of view, resulting in a pixel resolution of 2.43 microns. Table 1 provides more details of the images that make up the data set.

**Table 1.** Descriptors of the PCam images

Property	Value
Size	96 × 96
Channels	3 (BGR)
Bits per channel	8
Format	TIF

Figure 1 shows a sample labeled as positive, indicating that at least one pixel of the central region (32 × 32) contains tumor tissue. However, during the training of the network, the central region is not cropped and analyzed alone, as valuable information that helps in the generalization of the model could also be found at the edges.

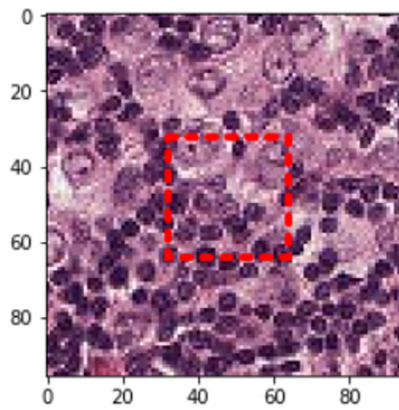


**Fig. 1.** Image labeled as positive samples [24]

The data set was divided into three segments. First, the test stage contains 10% of the total images. The training stage contains the remaining 90%, from which 10% is randomly taken for validation. The segmentation of the 220025 images is detailed in Table 2.

**Table 2.** Segmentation of data set

Total Images		220025	Training Images		198025	Images for Testing
Negative samples	Positive samples		Training images	Validation images		Number of images
130908	89117		178223	19802		22000

## 2.6 Image preprocessing

Data augmentation is a strategy to virtually increase the size of the training data set that makes the model more robust to slight changes in the input data.

This research applied random flip, random horizontal flip and random vertical flip techniques. These transformations are employed since breast lymph node tissue samples do not have an axis or reference point. In addition, it is common for the slides placed before the microscope to be rotated and inverted during analysis. Therefore, the application of the aforementioned techniques seeks to increase the samples in concordance similar to those that could be generated in a real environment.

### 3 RESULTS

#### 3.1 Considerations

Each model is trained in a separate programming environment, avoiding errors or compromising the veracity of the evaluation metrics. In order to obtain such metrics, multiple trainings are carried out by modifying the number of epochs, both for the first adjustment and for the final adjustment. The number of epochs defined for each test is presented in Table 3.

**Table 3.** Number of epochs used in each test

Test N°	CNN	First Tuning	Final Tuning
1	DenseNet-121	5 epochs	10 epochs
	DenseNet-169		
	DenseNet-201		
2	DenseNet-121	10 epochs	20 epochs
	DenseNet-169		
	DenseNet-201		
3	DenseNet-121	20 epochs	40 epochs
	DenseNet-169		
	DenseNet-201		

The search for learning rate and weight decays is run only once per model so that the CNNs start on equal footing during the first fit stage in all three tests performed. Figure 2 shows results from the learning rate and weight decay search. The values selected during the logarithmic scale search are shown in the Table 4.

**Table 4.** LR and WD found for the first fit

CNN	WD	Maximum LR
DenseNet-121	1e <sup>-2</sup>	5e <sup>-2</sup>
DenseNet-169	1e <sup>-4</sup>	4e <sup>-2</sup>
DenseNet-201	1e <sup>-4</sup>	3e <sup>-2</sup>

The final tuning only determines the new maximum learning rate for the second stage. We will obtain the value with the learning rate finder, as seen in Table 5. Additionally, the LR is much lower compared to the first adjustment as mentioned in [19].



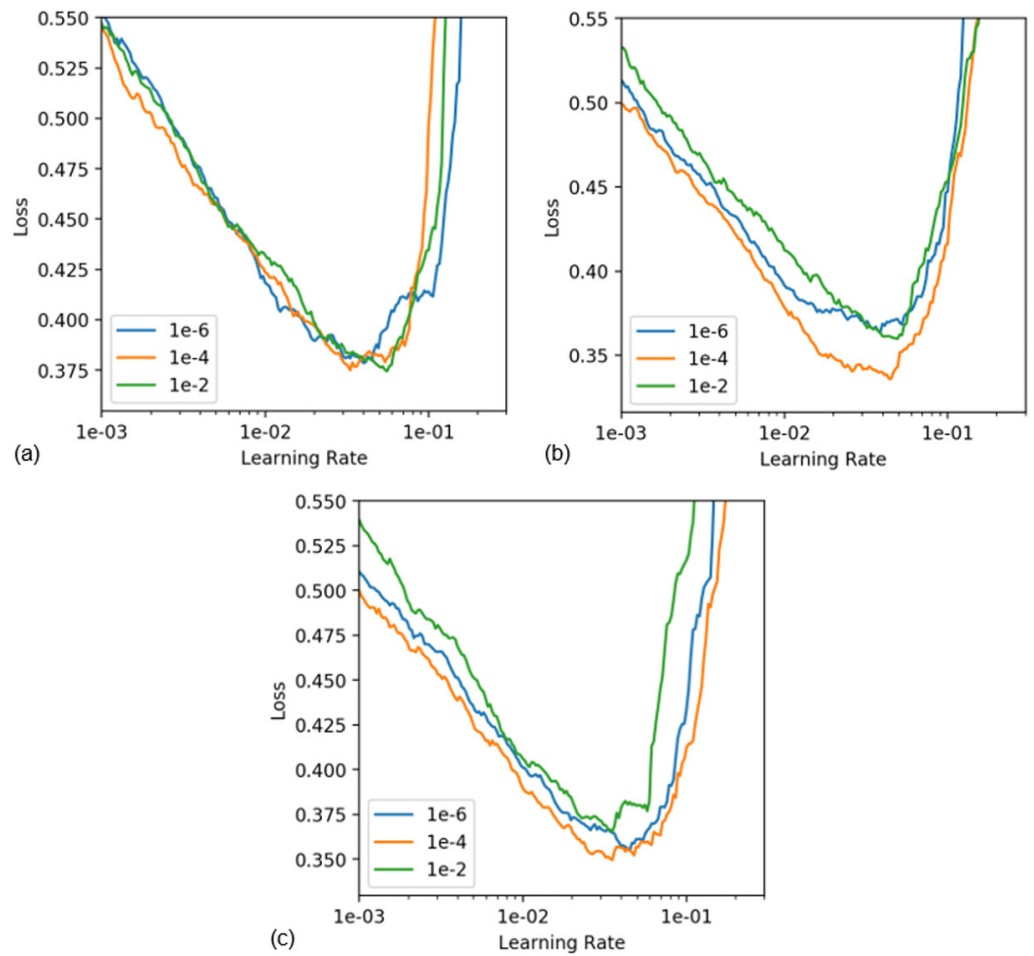


**Fig. 2.** LR and WD search results. (a) Result of DenseNet-121. (b) Result of DenseNet-169. (c) Result of DenseNet-201

**Table 5.** LR for final tuning

Test N°	CNN	WD	Maximum LR
1	DenseNet-121	1e <sup>-2</sup>	4e <sup>-4</sup>
	DenseNet-169	1e <sup>-4</sup>	6e <sup>-4</sup>
	DenseNet-201	1e <sup>-4</sup>	3e <sup>-4</sup>
2	DenseNet-121	1e <sup>-2</sup>	3e <sup>-4</sup>
	DenseNet-169	1e <sup>-4</sup>	3e <sup>-4</sup>
	DenseNet-201	1e <sup>-4</sup>	4e <sup>-4</sup>
3	DenseNet-121	1e <sup>-2</sup>	7e <sup>-4</sup>
	DenseNet-169	1e <sup>-4</sup>	1e <sup>-4</sup>
	DenseNet-201	1e <sup>-4</sup>	3e <sup>-4</sup>

### 3.2 Training

A set of 178223 different histopathological images were used for training and 19809 for validation. The accuracy achieved by the three models during the nine training sessions is detailed in Table 6.

**Table 6.** Comparison of validation accuracy

Test N°	CNN	First Tuning	Final Tuning
1	DenseNet-121	0.9459	0.9630
	DenseNet-169	0.9520	0.9689
	DenseNet-201	0.9515	0.9700
2	DenseNet-121	0.9482	0.9660
	DenseNet-169	0.9570	0.9748
	DenseNet-201	0.9584	0.9758
3	DenseNet-121	0.9464	0.9740
	DenseNet-169	0.9632	0.9755
	DenseNet-201	0.9648	0.9795

All models, after undergoing the first tuning, achieve classification of lymph node histopathological images with accuracy equal to or greater than 94%. Moreover, regardless of the increase in the number of epochs, the final tuning raises the efficiency of all models. Plots of training and validation losses obtained during final tuning are shown in Figures 3–5.

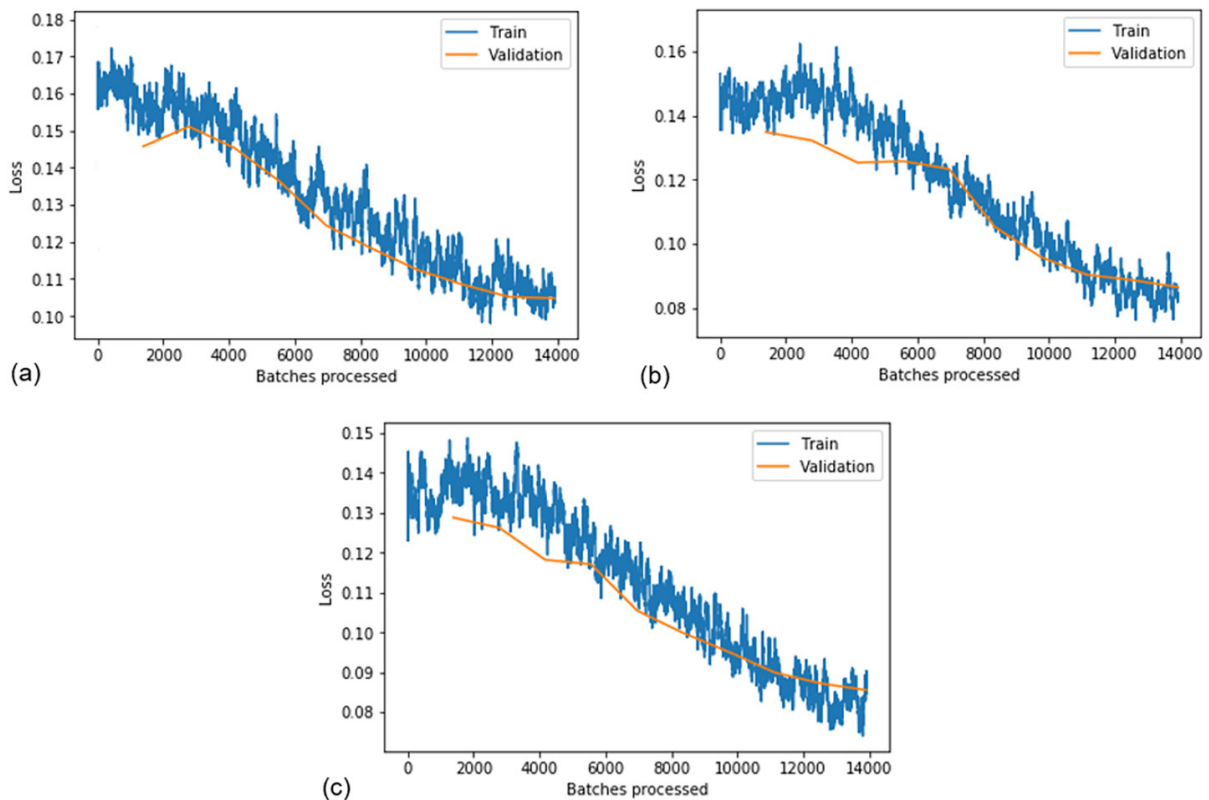


**Fig. 3.** First test. (a) Result of DenseNet-121. (b) Result of DenseNet-169. (c) Result of DenseNet-201



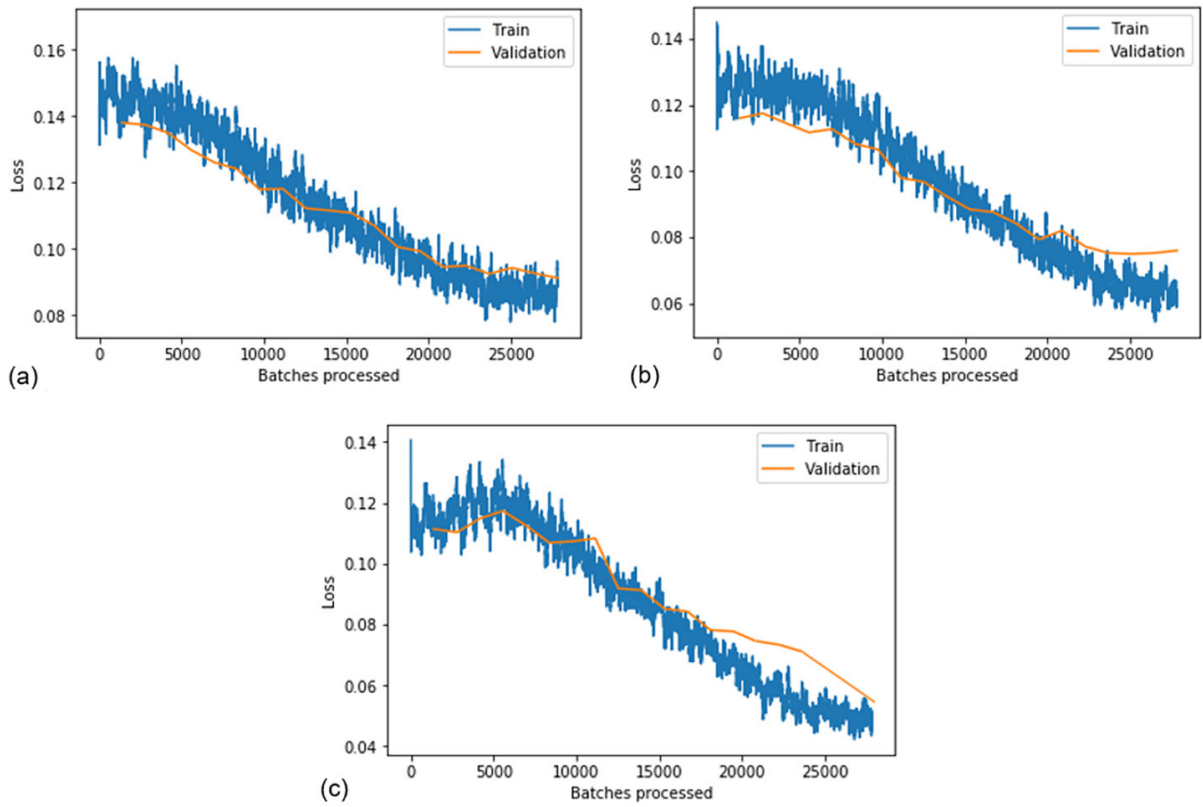


Fig. 4. Second test. (a) Result of DenseNet-121. (b) Result of DenseNet-169. (c) Result of DenseNet-201

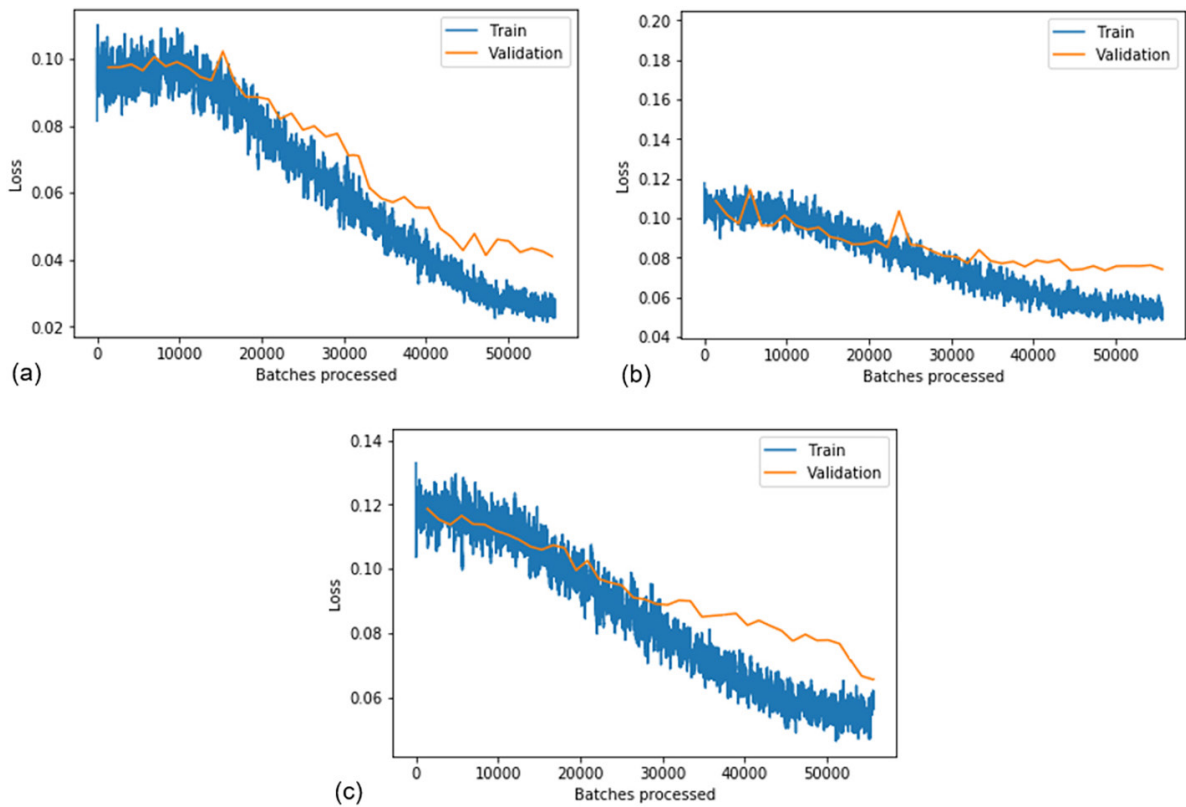


Fig. 5. Third test. (a) DenseNet-121 result. (b) Result of DenseNet-169. (c) Result of DenseNet-201

### 3.3 Prediction

After the training of each convolutional neural network, 22 thousand histopathological images, which were not part of the training or validation, are presented to the network so that it can perform the binary classification, this process is called prediction. Additionally, the evaluation of the performance of each model takes into account the confusion matrix, accuracy, precision, sensitivity, specificity, FDR, and F1.

### 3.4 First test

Figure 6 shows the confusion matrices obtained and Table 7 shows the metrics.

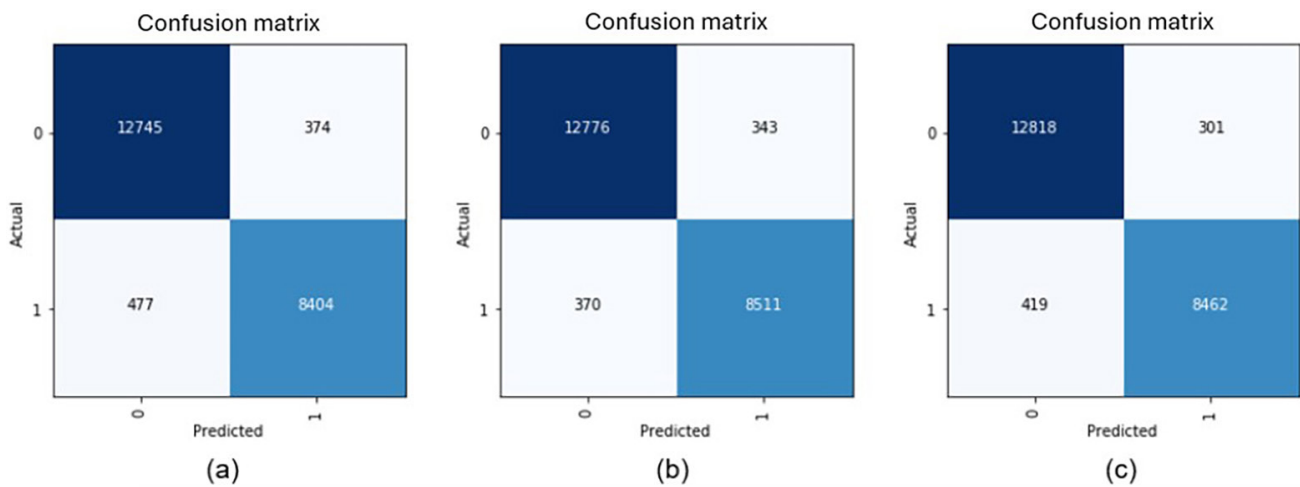


Fig. 6. Confusion matrices of the first test. (a) Result of DenseNet-121. (b) Result of DenseNet-169. (c) Result of DenseNet-201

Table 7. Evaluation metrics of the first test

CNN	Acc*	Pre**	Sen***	Spe****	FDR	F1
DenseNet-121	0.9613	0.9574	0.9463	0.9715	0.0426	0.9518
DenseNet-169	0.9676	0.9613	0.9583	0.9739	0.0387	0.9598
DenseNet-201	0.9673	0.9657	0.9528	0.9771	0.0343	0.9592

Notes: \*Accuracy; \*\*Precision; \*\*\*Sensibility; \*\*\*\*Specificity.

The best performance was obtained by DenseNet-169, reaching an accuracy of 96.73%. However, there is no noticeable difference between the three models.

### 3.5 Second test

As in the first test, the confusion matrices are obtained from the binary predictions of the three models, see Figure 7. The increase in the number of epochs also increases the training time with respect to the first test, but as shown in Table 8, the DenseNet-201 model improves its accuracy by 0.72% with respect to the last test. Nevertheless, the accuracy achieved by DenseNet-169 and DenseNet-201 is very similar.

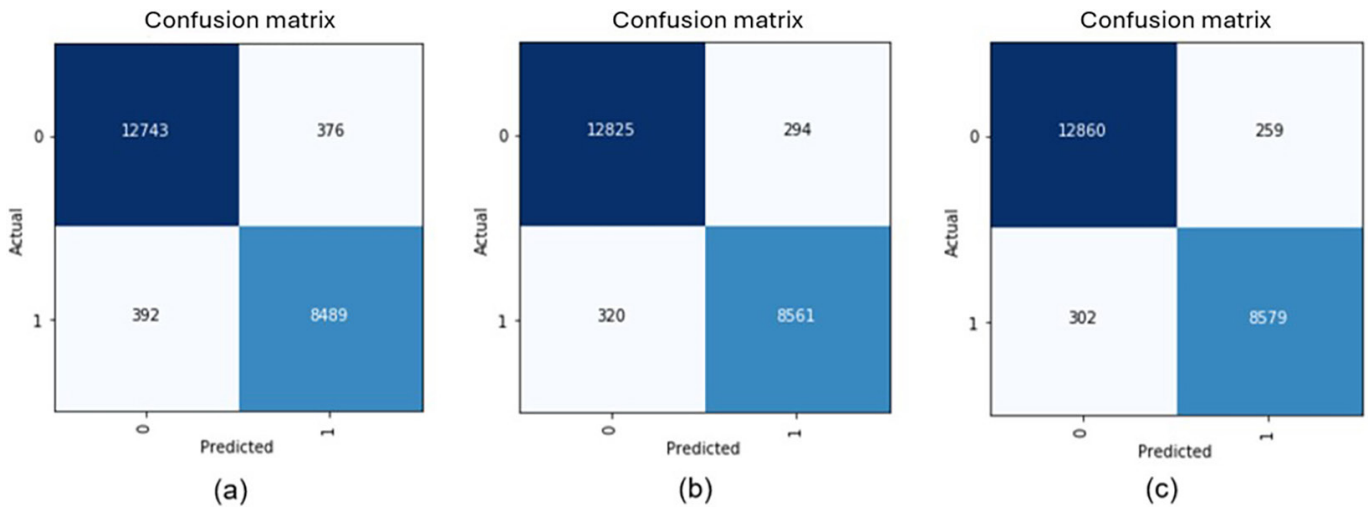


Fig. 7. Confusion matrices of the second test. (a) Result of DenseNet-121. (b) Result of DenseNet-169. (c) Result of DenseNet-201

Table 8. Evaluation metrics of the second test

CNN	Acc*	Pre**	Sen***	Spe****	FDR	F1
DenseNet-121	0.9651	0.9576	0.9559	0.9713	0.0424	0.9567
DenseNet-169	0.9721	0.9668	0.9640	0.9776	0.0332	0.9654
DenseNet-201	0.9745	0.9707	0.9660	0.9803	0.0293	0.9683

Notes: \*Accuracy; \*\*Precision; \*\*\*Sensibility; \*\*\*\*Specificity.

### 3.6 Third test

The number of epochs and training time are considerably increased for this third test. Figure 8 shows confusion matrices of the third test and Table 9 shows that the DenseNet-201 model has higher accuracy, since it misclassifies 455 out of 22000 images.

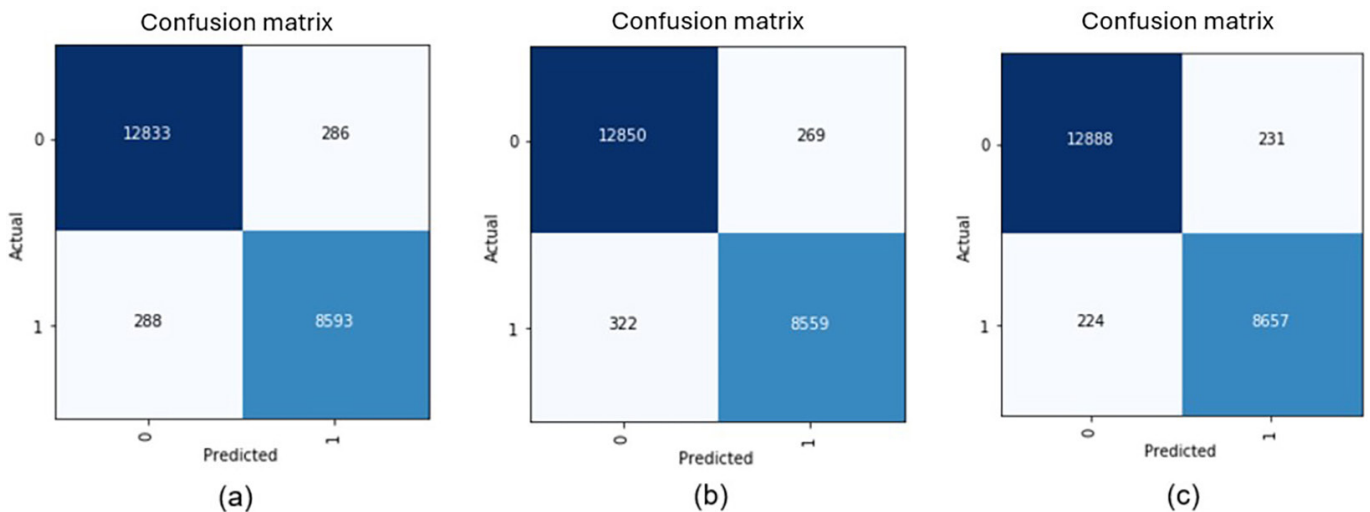


Fig. 8. Confusion matrices of the third test. (a) Result of DenseNet-121. (b) Result of DenseNet-169. (c) Result of DenseNet-201

**Table 9.** Evaluation metrics of the third test

CNN	Acc*	Pre**	Sen***	Spe****	FDR	F1
DenseNet-121	0.9739	0.9678	0.9676	0.9782	0.0322	0.9677
DenseNet-169	0.9731	0.9695	0.9637	0.9795	0.0305	0.9666
DenseNet-201	0.9793	0.9740	0.9748	0.9824	0.0260	0.9744

Notes: \*Accuracy; \*\*Precision; \*\*\*Sensibility; \*\*\*\*Specificity.

This last test identifies the best performance of DenseNet-201, outperforming the other models in all evaluation metrics. DenseNet-201 from the third test outperforms its sister models and itself from past tests. In Figure 9, we plot the ROC curve, obtaining a 99.69% area under the curve.

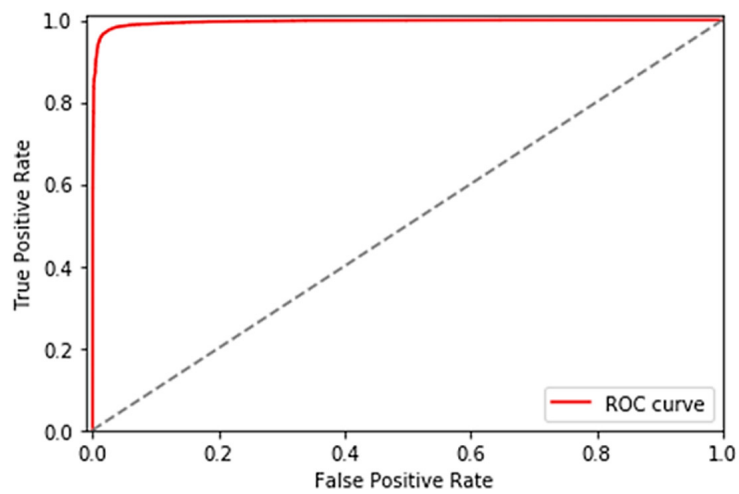


**Fig. 9.** ROC curve of DenseNet-201 in the third test

In Figure 9, the area under the curve is close to 1, implying that the model performance is optimal. The performance metrics obtained from the DenseNet-201 model of the third test are compared against the values presented in other studies employing a similar data set against. Finally, our proposed model shows better performance achieving accuracy, precision, sensitivity and F1 measure of 97.93%, 97.40%, 97.48% and 97.44%, respectively.

## 4 CONCLUSIONS

This manuscript proposes the use of convolutional neural networks for the binary classification of histopathological images of sentinel lymph nodes. In order to achieve the research objectives, each model was trained in two stages using the 1-cycle policy. Having completed the experimental tests and having used the evaluation metrics, we can conclude that the search for learning rate and weight decay simplified and optimized the training process of the models presented in this research. Additionally, the use of the 1-cycle policy improves the performance of the DenseNet architecture CNNs. Only 5 epochs of training are necessary to achieve an accuracy of approximately 95%.

On the other hand, two-stage training allows, in the second part, reducing the learning rate to increase the performance of the model without over tuning the network. Therefore, CNN networks are shown to be a potentially viable solution for binary classification of histopathological images of sentinel lymph nodes. DenseNet-201 achieves an accuracy of 97.93%, precision of 97.4%, false discovery rate of 2% and an area under the curve of 99.69% (see Table 10).

**Table 10.** Comparisons of the proposed method versus other methods

Models	Dataset	Acc*	Pre**	Sen***	F1
Our proposal	Kaggle	97.93%	97.40%	97.48%	97.44%
CNN-GRU [10]	Kaggle	97.10%	96.90%	96.87%	–
Resnet50 [25]	Kaggle	94.13%	–	–	–
VGG16 [25]	Kaggle	90.75%	–	–	–
CNN-GRU [26]	Kaggle	86.21%	–	85%	86%
SVM [27]	Kaggle	65%	–	64.90%	66%
CNN-6L [28]	PCam	73%	–	–	–
Resnet-50 with Densenet-201 [5]	ICPR 2014	84.8%	–	–	69.1%
ShuffleNet [29]	BreaKHis	96.94%	96.85%	96.70%	–
VGG16 [30]	BreaKHis	96.0%	96.0%	93.90%	–
DenseNet and SENet (IDSNet) [4]	BreaKHis	81.8%	–	–	–

Notes: \*Accuracy; \*\*Precision; \*\*\*Sensibility.

## 5 REFERENCES

- [1] H. G. Tani, L. Eloutouate, F. Elouaai, M. Bouhorma, and M. W. Hajoub, "Transforming healthcare: Leveraging vision-based neural networks for smart home patient monitoring," *International Journal of Online and Biomedical Engineering*, vol. 19, no. 10, pp. 20–32, 2023. <https://doi.org/10.3991/ijoe.v19i10.40381>
- [2] M. Arabahmadi, R. Farahbakhsh, and J. Rezazadeh, "Deep learning for smart healthcare—A survey on brain tumor detection from medical imaging," *Sensors*, vol. 22, no. 5, p. 1960, 2022. <https://doi.org/10.3390/s22051960>
- [3] X. Xu, M. An, J. Zhang, W. Liu, and L. Lu, "A high-precision classification method of mammary cancer based on improved DenseNet driven by an attention mechanism," *Computational and Mathematical Methods in Medicine*, vol. 2022, pp. 1–14, 2022. <https://doi.org/10.1155/2022/8585036>
- [4] X. Li, X. Shen, Y. Zhou, X. Wang, and T.-Q. Li, "Classification of breast cancer histopathological images using interleaved DenseNet with SENet (IDSNet)," *PLoS One*, vol. 15, no. 5, p. e0232127, 2020. <https://doi.org/10.1371/journal.pone.0232127>
- [5] T. Mahmood, M. Arsalan, M. Owais, M. B. Lee, and K. R. Park, "Artificial intelligence-based mitosis detection in breast cancer histopathology images using faster R-CNN and deep CNNs," *Journal of Clinical Medicine*, vol. 9, no. 3, p. 749, 2020. <https://doi.org/10.3390/jcm9030749>
- [6] S. Iqbal and A. N. Qureshi, "A heteromorphous deep CNN framework for medical image segmentation using local binary pattern," *IEEE Access*, vol. 10, pp. 63466–63480, 2022. <https://doi.org/10.1109/ACCESS.2022.3183331>

- [7] M. J. Umer, M. Sharif, S. Kadry, and A. Alharbi, "Multi-class classification of breast cancer using 6B-Net with deep feature fusion and selection method," *Journal of Personalized Medicine*, vol. 12, no. 5, p. 683, 2022. <https://doi.org/10.3390/jpm12050683>
- [8] R. Schmitz *et al.*, "Multi-scale fully convolutional neural networks for histopathology image segmentation: From nuclear aberrations to the global tissue architecture," *Medical Image Analysis*, vol. 70, p. 101996, 2021. <https://doi.org/10.1016/j.media.2021.101996>
- [9] Y. Ektefaie *et al.*, "Integrative multiomics-histopathology analysis for breast cancer classification," *NPJ Breast Cancer*, vol. 7, no. 1, p. 147, 2021. <https://doi.org/10.1038/s41523-021-00357-y>
- [10] S. Ahmad *et al.*, "A novel hybrid deep learning model for metastatic cancer detection," *Computational Intelligence and Neuroscience*, vol. 2022, pp. 1–14, 2022. <https://doi.org/10.1155/2022/8141530>
- [11] D. S. Acharya, K. Eashwer, S. S. Kumar, R. Sivakumar, P. C. Kishoreraja, and R. Srinivasagan, "Multiple disease detection using machine learning techniques," *International Journal of Online and Biomedical Engineering*, vol. 19, no. 13, pp. 120–137, 2023. <https://doi.org/10.3991/ijoe.v19i13.40523>
- [12] A. Johny and K. N. Madhusoodanan, "Dynamic learning rate in deep CNN model for metastasis detection and classification of histopathology images," *Computational and Mathematical Methods in Medicine*, vol. 2021, pp. 1–13, 2021. <https://doi.org/10.1155/2021/5557168>
- [13] A. E. Ilesanmi and T. O. Ilesanmi, "Methods for image denoising using convolutional neural network: A review," *Complex & Intelligent Systems*, vol. 7, no. 5, pp. 2179–2198, 2021. <https://doi.org/10.1007/s40747-021-00428-4>
- [14] M. D. Swetha and C. R. Aditya, "Noise invariant convolution neural network for segmentation of multiple sclerosis lesions from brain magnetic resonance imaging," *International Journal of Online and Biomedical Engineering*, vol. 18, no. 13, pp. 38–55, 2022. <https://doi.org/10.3991/ijoe.v18i13.34273>
- [15] J. Xie, R. Liu, J. Luttrell, and C. Zhang, "Deep learning based analysis of histopathological images of breast cancer," *Frontiers in Genetics*, vol. 10, 2019. <https://doi.org/10.3389/fgene.2019.00080>
- [16] Ş. Öztürk and B. Akdemir, "Effects of histopathological image pre-processing on convolutional neural networks," *Procedia Computer Science*, vol. 132, pp. 396–403, 2018. <https://doi.org/10.1016/j.procs.2018.05.166>
- [17] B. Kieffer, M. Babaie, S. Kalra, and H. R. Tizhoosh, "Convolutional neural networks for histopathology image classification: Training vs. Using pre-trained networks," in *2017 Seventh International Conference on Image Processing Theory, Tools and Applications (IPTA)*, IEEE, 2017, pp. 1–6. <https://doi.org/10.1109/IPTA.2017.8310149>
- [18] G. Huang, Z. Liu, L. Van Der Maaten, and K. Q. Weinberger, "Densely connected convolutional networks," in *2017 IEEE Conference on Computer Vision and Pattern Recognition (CVPR)*, IEEE, 2017, pp. 2261–2269. <https://doi.org/10.1109/CVPR.2017.243>
- [19] L. N. Smith, "A disciplined approach to neural network hyper-parameters: Part 1 – learning rate, batch size, momentum, and weight decay," arXiv preprint arXiv:1803.09820, 2018.
- [20] L. N. Smith, "Cyclical learning rates for training neural networks," in *2017 IEEE Winter Conference on Applications of Computer Vision (WACV)*, IEEE, 2017, pp. 464–472. <https://doi.org/10.1109/WACV.2017.58>
- [21] G. Van Rossum and F. L. Drake, *Python 3 Reference Manual*. Scotts Valley: CreateSpace, 2009.
- [22] J. Howard and S. Gugger, "Fastai: A layered API for deep learning," *Information*, vol. 11, no. 2, p. 108, 2020. <https://doi.org/10.3390/info11020108>
- [23] A. Paszke *et al.*, "PyTorch: An imperative style, high-performance deep learning library," arXiv preprint arXiv:1912.01703v1, 2019.



- [24] W. Cukierski, "Histopathologic cancer detection," Kaggle. <https://kaggle.com/competitions/histopathologic-cancer-detection>
- [25] J. Abdollahi, N. Davari, Y. Panahi, and M. Gardaneh, "Detection of metastatic breast cancer from whole-slide pathology images using an ensemble deep-learning method," *Archives of Breast Cancer*, pp. 364–376, 2022. <https://doi.org/10.32768/abc.202293364-376>
- [26] X. Wang *et al.*, "Intelligent hybrid deep learning model for breast cancer detection," *Electronics (Basel)*, vol. 11, no. 17, p. 2767, 2022. <https://doi.org/10.3390/electronics11172767>
- [27] M. Waddell, D. Page, and J. Shaughnessy, "Predicting cancer susceptibility from single-nucleotide polymorphism data," in *Proceedings of the 5th International Workshop on Bioinformatics*, New York, NY, USA: ACM, 2005, pp. 21–28. <https://doi.org/10.1145/1134030.1134035>
- [28] E. Bonnet, "Using convolutional neural networks for the classification of breast cancer images," arXiv preprint arXiv:2108.13661, 2021.
- [29] H. Aljuaid, N. Alturki, N. Alsubaie, L. Cavallaro, and A. Liotta, "Computer-aided diagnosis for breast cancer classification using deep neural networks and transfer learning," *Computer Methods and Programs in Biomedicine*, vol. 223, p. 106951, 2022. <https://doi.org/10.1016/j.cmpb.2022.106951>
- [30] D. Albashish, R. Al-Sayyed, A. Abdullah, M. H. Ryalat, and N. Ahmad Almansour, "Deep CNN model based on VGG16 for breast cancer classification," in *2021 International Conference on Information Technology (ICIT)*, IEEE, 2021, pp. 805–810. <https://doi.org/10.1109/ICIT52682.2021.9491631>

## 6 AUTHORS

**Diego Alberto Cadillo-Laurentt** is a Peruvian electronic engineer, he obtained a bachelor's degree in electronic engineering from Universidad Tecnológica del Perú in 2023. He has been an intern at Siemens Healthineers for 2 years (E-mail: [1611744@utp.edu.pe](mailto:1611744@utp.edu.pe)).

**Ernesto Alonso Paiva-Peredo** received the title of Electrical Mechanical Engineer from the University of Piura, Peru, in 2013. He has completed a master's degree in electrical mechanical engineering with a mention in Automation and Optimization at the University of Piura funded by CONCYTEC 2016. He was a research assistant at the Department of Technology and Innovation (DTI) – SUPSI. Now, he is a Professor-Researcher at Universidad Tecnológica del Perú (E-mail: [epaiva@utp.edu.pe](mailto:epaiva@utp.edu.pe)).